Regulation of blood cell transdifferentiation by oxygen sensing neurons

Sean Corcoran[2], Anjeli Mase[2], Yousuf Hashmi[2], Debra Ouyang[2], Jordan Augsburger[2], Thea Jacobs[2], Katelyn Kukar[2], Katja Brückner[1, 2, 3, 4]

[1]Eli and Edythe Broad Center of Regeneration Medicine and Stem Cell Research

[2]Department of Cell and Tissue Biology

[3]Cardiovascular Research Institute, University of California San Francisco, San Francisco, CA

[4] Corresponding Author:

35 Medical Center Way

San Francisco, CA 94143-0669

email: katja.brueckner@ucsf.edu

Highlights

- Functional lineage tracing reveals in vivo transdifferentiation in a *Drosophila* model of hematopoiesis
- Active sensory neurons of the caudal sensory cones promote blood cell transdifferentiation in the *Drosophila* larva
- Environmental oxygen sensing and atypical guanylyl cyclase activity in sensory cone neurons drive blood cell transdifferentiation

Keywords

Drosophila melanogaster, transdifferentiation, hematopoiesis, microenvironment, hemocyte, macrophage, plasmatocyte, crystal cell, sensory neurons, sensory cones, atypical guanylyl cyclase, oxygen sensing, hypoxia

Summary

Transdifferentiation generates specialized cell types independent of stem or progenitor cells. Despite the unique process, it remains poorly understood how transdifferentiation is regulated in vivo. Here we reveal a mechanism of environmental control of blood cell transdifferentiation in a *Drosophila* model of hematopoiesis. Functional lineage tracing provides evidence for transdifferentiation from macrophage-like plasmatocytes to crystal cells that execute melanization. Interestingly, this transdifferentiation is promoted by neuronal activity of a specific subset of sensory neurons, in the caudal sensory cones of the larva. Crystal cells develop from plasmatocyte clusters surrounding the sensory cones, triggered by environmental conditions: oxygen sensing, and the atypical guanylyl cyclase Gyc88E specifically expressed in the sensory cone neurons, drive plasmatocyte-to-crystal cell transdifferentiation. Our findings reveal an unexpected functional and molecular link of environment-monitoring sensory neurons that govern blood cell transdifferentiation in vivo, suggesting similar principles in vertebrate systems where environmental sensors and blood cell populations coincide.

Introduction

A Drosophila model of blood cell transdifferentiation

The phenomenon of transdifferentiation has been noted in a variety of species (Cieslar-Pobuda et al., 2017; Graf, 2011; Reid and Tursun, 2018), yet its in vivo regulation remains poorly understood. In the vertebrate blood cell system, reports of transdifferentiation have for the most part been limited to cell culture systems and experimental manipulations. For example, C/EBP (CCAAT/enhancer-binding protein) transcription factors drive transdifferentiation of vertebrate B cells to macrophages (Di Tullio et al., 2011; Xie et al., 2004), B lymphoma and leukemia cell lines to macrophages (Rapino et al., 2013), and B cells to Granulocyte-Macrophage Precursors (Cirovic et al., 2017). Similarly, manipulation of key transcription factors such as FLI1 and ERG results in transdifferentiation of erythroblasts to megakaryocytes (Siripin et al., 2015), and deletion of the BAF Chromatin Remodeling Complex Subunit Bcl11b triggers T cell transition to NK cells (Li et al., 2010). Transdifferentiation of lymphoid and myeloid cells has been modeled mathematically (Collombet et al., 2017). However, in vivo, the underlying cellular and molecular mechanisms of blood cell transdifferentiation during development and homeostasis and the role of the environment remain elusive.

To investigate principles of in vivo transdifferentiation in the hematopoietic system, we turned to a model in *Drosophila melanogaster*. *Drosophila* offers proven parallels to the two major lineages that produce myeloid blood cells in vertebrates (Davies et al., 2013; Perdiguero and Geissmann, 2016; Sieweke and Allen, 2013), with its two myeloid lineages of blood cells, or hemocytes (Gold and Brückner, 2014, 2015; Holz et al., 2003), (1) the embryonic lineage of hemocytes that proliferate as differentiated cells in hematopoietic pockets of the larval body wall, and resemble vertebrate tissue macrophages, and (2) the progenitor-based lymph gland lineage (Banerjee et al., 2019). Both *Drosophila* blood cell lineages produce at least three differentiated blood cell types: macrophage-like plasmatocytes, crystal cells that mediate melanization, and lamellocytes, large immune cells specialized for encapsulation (Banerjee et al., 2019; Gold and Brückner, 2014, 2015). During larval stages, embryonic-lineage plasmatocytes show signs of fate changes to other blood cell types: Transdifferentiation to lamellocytes occurs in response to immune challenges (Markus et al., 2009), and transdifferentiation to crystal cells was suggested even under steady state conditions (Leitao and Sucena, 2015). However, it remains unclear what are the anatomical requirements and environmental inputs that regulate plasmatocyte-to-crystal cell transdifferentiation in vivo. Hematopoietic sites of

45 the *Drosophila* larva contain sensory neuron clusters of the peripheral nervous system (PNS) that
46 serve as microenvironments for plasmatocyte survival, proliferation and localization (Gold and
47 Brückner, 2014, 2015; Makhijani et al., 2017; Makhijani et al., 2011; Makhijani and Brückner, 2012).
48 Considering this, we investigated the role of these specialized hematopoietic pockets in hemocyte
49 transdifferentiation.

50

51 **Results**

52 *Phagocytic plasmatocytes transdifferentiate to crystal cells*

53 First we examined the formation of crystal cells and their anatomical locations during larval
54 development. We quantified crystal cells using a traditional way of labeling crystal cells based on
55 their expression of prophenoloxidases (Corcoran and Brückner, 2020; Rizki and Rizki, 1959),
56 enzymes responsible for melanization, the main immune function of crystal cells (Bidla et al., 2009;
57 Dudzic et al., 2015; Lu et al., 2014). Induction of melanization blackens crystal cells (Corcoran and
58 Brückner, 2020; Rizki and Rizki, 1959) and marks similar cell populations as the crystal cell reporter
59 *lozenge-GAL4* (*lz-GAL4; UAS-GFP*) (SupplFig. 1 A, B). During larval development, crystal cell
60 numbers increase slowly over the first and second larval instar stages, but expand more rapidly
61 during the third instar stage (Fig. 1 A), largely mirroring the exponential increase of plasmatocytes
62 during larval development (Fig 1 B) (Makhijani et al., 2011; Petraki et al., 2015). To visualize the
63 locations of crystal cells and plasmatocytes, we coexpressed two fluorescent protein reporters (for
64 crystal cells *BcF2-GFP* (Tokusumi et al., 2009), and for plasmatocytes *Hml*Δ*-DsRed* (Makhijani et
65 al., 2011)). Interestingly, crystal cells are strongly enriched in a cluster in the terminal segment of the
66 *Drosophila* larva, a region where plasmatocytes are also known to accumulate (Fig. 1 C-C'', D-D')
67 (Makhijani et al., 2011). Crystal cells are occasionally also found in other hematopoietic pockets, and
68 in dorsal vessel-associated clusters where floating hemocytes accumulate (Cevik et al., 2019; Petraki
69 et al., 2015).

70 Since previous studies suggested plasmatocyte-to-crystal cell transdifferentiation solely based on live
71 imaging (Leitao and Sucena, 2015), we sought an independent functional lineage tracing approach.
72 Asking whether crystal cells derive from undifferentiated progenitors or differentiated,
73 phagocytically active plasmatocytes, we traced cells based on the unique ability of differentiated
74 plasmatocytes to phagocytically uptake fluorescently labeled beads (Fig. 1 E-E'''). We injected
75 *Drosophila* larvae expressing fluorescent reporters for plasmatocytes and crystal cells with blue

76 fluorescent latex beads. Injected larvae were incubated in a time course, followed by the release of
77 hemocytes and quantification of the relative fractions of phagocytosis-labeled plasmatocytes and -
78 crystal cells (Fig. 1 F, G). The fraction of blue bead positive plasmatocytes quickly reached saturation
79 (~50% at 1h, ~90% at 4h and 22h). In contrast, crystal cells were labeled by blue beads with a
80 significant time delay (<10% at 1h, ~ 50% at 4h, ~70% at 22h) (Fig. 1 G). Together with previous
81 reports that suggested crystal cells are not capable of phagocytosis or proliferation (Lanot et al., 2001;
82 Leitao and Sucena, 2015; Tattikota et al., 2019) this supports a model of plasmatocyte-to-crystal cell
83 transdifferentiation, in which crystal cells derive from phagocytically active plasmatocyes, rather than
84 from undifferentiated, phagocytosis-incompetent progenitors.

85 *Sensory neuron activity promotes crystal cell transdifferentiation*

86 Next, we investigated the anatomical locations of crystal cells and plasmatocytes relative to sensory
87 neurons, using fluorescent reporters and live imaging, including the sensory neuron specific driver
88 *21-7-GAL4, UAS-CD8-GFP* (Song et al., 2007) (Fig. 2 A). We found that both plasmatocytes and
89 crystal cells colocalize with sensory neurons, with one important difference: plasmatocytes are found
90 in all hematopoietic pockets (Fig. 2 A), while crystal cells are mainly localized in the terminal
91 hematopoietic pocket of the larva (Fig. 2 B).

92 Given this colocalization with sensory neurons, we asked whether sensory neuron activity has an
93 effect on crystal cell generation. To mimic activation of sensory neurons, we exposed larvae to the
94 acetylcholine receptor agonist carbamoycholine (carbachol). Carbachol exposure over 4 hours
95 resulted in a moderate increase of crystal cell numbers (Fig. 2 C). More specifically and
96 complementary to this, we silenced sensory neurons by transient expression of *Kir2.1*, an inward
97 rectifying K+ channel that causes neuron hyperpolarization (Baines et al., 2001). Interestingly, *Kir2.1*
98 expression over 22 hours caused a dramatic drop in crystal cell numbers (Fig. 2 D). There was no
99 significant effect of neuronal silencing on total hemocyte numbers under comparable conditions
100 (SupplFig. 2 and (Makhijani et al., 2017)). To address whether sensory neuron silencing by Kir2.1
101 affects plasmatocyte to crystal cell transdifferentiation, we performed phagocytosis lineage tracing.
102 Indeed, transient neuronal silencing affects the fraction of crystal cells derived from blue bead labeled
103 plasmatocytes, while the ability of plasmatocytes to phagocytose remains the same (Fig. 2 E, F).
104 Taken together, our findings suggest that sensory neuron activity promotes transdifferentiation of
105 plasmatocytes to crystal cells.

106

107 *Crystal cells colocalize with, and require, sensory neurons of the sensory cones*

108 To gain more insight, we focused on the caudal cluster of crystal cells. Closer inspection of combined
109 fluorescent reporters for crystal cells and sensory neurons showed that crystal cells colocalize
110 particularly well with sensory organs of the sensory cones (Fig. 3 A-A'' and C-D''), protruding
111 structures that are grouped around the posterior spiracles, the terminal tubes of the tracheal system
112 (Hayashi and Kondo, 2018; Kuhn et al., 1992). Plasmatocytes accumulate in a large cluster around
113 the sensory cones already in the 2nd instar larva (Fig. 3 B-B''), which seems to foreshadow the pattern
114 and abundance of crystal cells in the 3rd instar larva (Fig. 3 D-D''). We therefore hypothesized that
115 many plasmatocytes of the 2nd instar larva may transdifferentiate to crystal cells, as is apparent in the
116 3rd instar.

117 Given the intriguing colocalization of crystal cells and sensory neurons and the dependence of blood
118 cell transdifferentiation on neuronal activity, we investigated the specific requirement of sensory cone
119 neurons for crystal cell production. A group of genes specifically expressed in sensory cone neurons
120 are atypical guanylyl cyclases, *Gyc88E*, *Gyc89Da*, and *Gyc89Db* (Vermehren-Schmaedick et al.,
121 2010). Using the driver *Gyc89Db-GAL4* (Vermehren-Schmaedick et al., 2010) (Fig. 3 E, F), we
122 ablated sensory cone neurons by transiently expressing the proapoptotic gene *head involution defect*
123 *(Hid)* in its non-repressible version (*Hid* ^{ala5}) (Bergmann et al., 2002). Ablation of sensory cone
124 neurons did not affect larval viability, but it strongly reduced crystal cell numbers (Fig. 3 G).
125 Conversely, ectopic activation of sensory cone neurons by specific expression and transient induction
126 of the heat-induced cation channel TrpA1 (Hamada et al., 2008) caused a significant increase in
127 crystal cells (Fig. 3 H). Taken together, we conclude that crystal cells and their precursor
128 plasmatocytes are strongly enriched at the sensory cones of the larva. Sensory cone neurons, and their
129 activity, are required for crystal cells.

130 *Oxygen sensing through atypical guanylyl cyclases drives plasmatocyte-to-crystal cell*
131 *transdifferentiation*

132 The atypical guanylyl cyclase Gyc88E is a cytoplasmic oxygen sensor that acts as homodimer or
133 forms heterodimers with related guanylyl cyclases such as Gyc89Da or Gyc89Db, (Huang et al.,
134 2007; Morton, 2004; Morton et al., 2005; Vermehren et al., 2006). Gyc88E complexes, which are
135 active already at ambient oxygen levels, generate the second messenger cyclic GMP (cGMP) that in
136 turn activates neurons (Morton, 2004; Morton et al., 2008). Since we found that sensory cone neurons
137 expressing these Gycs are required for crystal cell formation, we decided to test Gyc function itself in

relation to crystal cell transdifferentiation. When the obligatory subunit, Gyc88E, was silenced in the sensory cone neurons, crystal cell numbers were reduced (Fig. 4 A). Phagocytosis lineage tracing confirmed that Gyc88E function is required for transdifferentiation of plasmatocytes to crystal cells, as the fraction of crystal cells carrying blue beads was significantly reduced in *Gyc88E* RNAi knockdowns, while phagocytosis by plasmatocytes remained the same (Fig. 4 B). Given the role of Gycs as oxygen sensors, we next investigated the effect of varying atmospheric oxygen concentrations on crystal cell formation. Assessing crystal cell numbers per larva as readout, we exposed larvae to reduced levels of oxygen (8%, or 5%) for 6 hours. Compared to normoxia (~21% oxygen), 8% hypoxia caused mild reduction in crystal cells and 5% oxygen caused a significant drop in crystal cells, while total hemocyte numbers remained unaffected (SupplFig. 3 A, B, Fig. 4 C). Following up on the robust results obtained under 5% oxygen, we determined whether hypoxia affects blood cell transdifferentiation, performing phagocytosis lineage tracing for 6 hours under hypoxic conditions (5% O_2) and normoxia. Interestingly, hypoxia phenocopies silencing of Gyc88E function in sensory cone neurons, resulting in a significant reduction of blue beads in crystal cells, while phagocytosis levels of plasmatocytes remain unaffected (Fig. 4 D). Our data demonstrate a role for oxygen and the atypical guanylyl cyclase Gyc88E, likely though its link to activation of the sensory cone neurons, in the promotion of plasmatocyte-to-crystal cell transdifferentiation (Fig. 4 E). This model supports the kinetics of crystal cells following plasmatocyte expansion, based on the transition of plasmatocytes to crystal cells in particular in the proximity of sensory cone neurons (SupplFig. 4 A).

Discussion

Our work has identified an unexpected mechanistic link between oxygen sensing and blood cell transdifferentiation, which is facilitated through a particular set of sensory neurons and an intracellular atypical guanylyl cyclase. This new paradigm inspires the search for similar principles of neuronally controlled blood cell transdifferentiation that responds to environmental conditions in other species including humans.

Transdifferentiation results in the conversion of one differentiated cell type to another. In some systems, new differentiated cell types arise after de-differentiation to a transient pluripotent intermediate (Graf, 2011; Pesaresi et al., 2019; Reid and Tursun, 2018). Our work supports a model of direct transdifferentiation based on fluorescent reporters and phagocytosis lineage tracing.

169 Independent approaches also support a model of continuous blood cell transdifferentiation from
170 plasmatocytes to crystal cells through progressive states, based on single cell RNAseq pseudotime
171 lineage analysis (Tattikota et al., 2019). Transdifferentiation may be the fastest and most efficient
172 way for animals to shape the composition of their blood cell pool according to environmental
173 conditions such as oxygen levels and potentially other inputs.

174 Gyc intracellular oxygen sensors mediate oxygen detection in sensory neurons (Vermehren et al.,
175 2006), similar to other oxygen sensing mechanisms known in vertebrate neurons and other sensory
176 cells (Caravagna and Seaborn, 2016; Pokorski et al., 2016). In contrast, HIF (hypoxia inducible
177 factor) transcription factors regulate target genes in response to low oxygen conditions in a variety of
178 cell types (Gorr et al., 2006; Majmundar et al., 2010). Hypoxia, through HIF, regulates mammalian
179 hematopoiesis, lymphopoiesis and erythropoiesis (Chabi et al., 2019; Haase, 2013; Imanirad and
180 Dzierzak, 2013). The *Drosophila* HIF1a *sima* (*similar*) plays a role in crystal cell formation in the
181 *Drosophila* lymph gland (Mukherjee et al., 2011), however this effect is independent of HIF1β and
182 hypoxia target genes. Instead, formation of *Drosophila* crystal cells has been linked to Notch
183 signaling at various developmental stages (Duvic et al., 2002; Krzemien et al., 2007; Lebestky et al.,
184 2000; Lebestky et al., 2003; Leitao and Sucena, 2015; Mukherjee et al., 2011). It remains to be
185 determined whether oxygen sensing neurons and/or the signal receiving plasmatocytes are connected
186 to Notch signaling or an independent pathway that governs the fate switch of plasmatocytes to crystal
187 cells.

188 Linking oxygen sensing to crystal cell formation via neuronal activity involves Gyc88E and likely
189 additional factors that modulate its activity under long-term hypoxia. While hypoxia in the range of
190 minutes enhances Gyc88E activity and induces short-term behavioral responses in *Drosophila* larvae,
191 additional regulatory factors such as nitric oxide (NO) are known to dampen Gyc88E activity (Huang
192 et al., 2007) and could be responsible for the reduction in crystal cell transdifferentiation we observe.
193 Interestingly, NO is known to be induced by long-term hypoxia and shows particularly high levels in
194 the sensory cones (Wingrove and O'Farrell, 1999). Additionally or alternatively, long-term hypoxia
195 could affect Gyc88E activity through refractory mechanisms, interaction with additional regulatory
196 interaction partners (Ding et al., 2020), links to alternative downstream effectors, or even alternative
197 function. Under short-term hypoxia, Gycs generate cGMP which acts through the cyclic nucleotide
198 gated channel A (CNGA) (Morton et al., 2008; Vermehren-Schmaedick et al., 2010). CNG channels
199 mediate influx of calcium ions, among others, resulting in consecutive activation of
200 calmodulin/CaMK signaling and sensory transduction (Kaupp and Seifert, 2002; Pifferi et al., 2006).

While it is difficult to determine the effects of short-term hypoxia on the comparably slow process of blood cell transdifferentiation, the key steps of signaling downstream of Gyc88E in blood cell transdifferentiation and the quantitative and/or qualitative differences of signaling under conditions of long-term hypoxia remain to be seen.

Regulation of blood cell transdifferentiation by sensory cone neurons offers advantages of immediate sensitivity and may further integrate the response to a variety of environmental conditions. Sensory cone neurons are in contact with the surrounding atmosphere, based on social burying during feeding in which larvae expose their caudal ends with the sensory cones, a behavior that also allows air intake to the tracheal system through the neighboring posterior spiracles (Hayashi and Kondo, 2018; Wu et al., 2003) (SupplFig. 4 B), and when larvae eventually exit the food source to pupariate (Wu et al., 2003) (SupplFig. 4 B). With their exposed nature, these sensory neurons may also integrate other inputs such as chemical cues or even light from the environment (Stewart et al., 2015; Vermehren-Schmaedick et al., 2011; Xiang et al., 2010).

Neuronal regulation of the hematopoietic system and other organs is an important paradigm in biology, which is starting to come to light in a variety of species (Kumar and Brockes, 2012). In *Drosophila,* neuronal regulation of hematopoiesis is well established. Embryonic-lineage plasmatocytes depend on sensory neurons for their survival, proliferation and localization (Gold and Brückner, 2014, 2015; Makhijani et al., 2017; Makhijani et al., 2011; Makhijani and Brückner, 2012). Activin-β, a TGF-β family ligand, is a key signal produced by active sensory neurons that promotes plasmatocyte proliferation and adhesion (Makhijani et al., 2017). Identification of the signal/s from active sensory cone neurons that trigger transdifferentiation will be the focus of intense future study. We postulate secreted factor/s, which could potentially, albeit at reduced efficiency, also act at a distance, promoting transdifferentiation of smaller numbers of crystal cells in the dorsal vessel associated hemocyte clusters (Leitao and Sucena, 2015) and segmental hematopoietic pockets. In this context it is interesting to note that in long term memory formation, Activin expression is induced downstream of calmodulin/CaMK/CREB signaling in both *Drosophila* and vertebrates (Inokuchi et al., 1996; Miyashita et al., 2012), suggesting potential parallels of this signaling cassette in neuron-induced blood cell transdifferentiation.

In vertebrates, functional links of hematopoiesis with sensory neurons or other sensing systems remain largely unknown, despite some aspects of bone marrow hematopoiesis and inflammatory responses being regulated by the autonomic nervous system (Hanoun et al., 2015; Pavlov and Tracey,

232 2012). Oxygen sensing could be an important regulatory factor in recently identified hematopoietic
233 sites such as the vertebrate lung, which provides a microenvironment for limited blood cell
234 progenitors and megakaryocytes that are active in platelet production (Lefrancais et al., 2017; Martin
235 et al., 1983). The lung, like many other organs, also harbors tissue macrophages that proliferate in
236 local microenvironments and bear evolutionary parallels with *Drosophila* embryonic-lineage
237 plasmatocytes (Gold and Brückner, 2014, 2015; Perdiguero and Geissmann, 2016). Interestingly, the
238 lung and airways are rich in vagal afferent nerves that sense chemical and mechanical cues (Chang et
239 al., 2015; Mazzone and Undem, 2016), and neuroendocrine cells of the lung that sense oxygen early
240 in life and later provide a microenvironment for airway epithelial cells (Caravagna and Seaborn,
241 2016; Cutz et al., 2007). Investigation of sensory neurons and other sensors may therefore open a new
242 chapter in the regulation of vertebrate hematopoiesis, transdifferentiation, and immune cell fate and
243 function.

244

245 **Materials and Methods**

246 *Drosophila Strains*

247 *Drosophila* drivers, reporters and related lines used were *HmlΔ-GAL4, UAS-GFP* (Sinenko and
248 Mathey-Prevot, 2004)*;* combination driver *HmlΔGAL4, UAS-GFP; He-GAL4* (Yang et al., 2015)
249 (gift from Dan Hultmark), *lz-GAL4; UAS-GFP* (J. Pollock, Bloomington), *21-7-GAL4* (Makhijani et
250 al., 2011; Song et al., 2007) *Gyc89Db-GAL4 (Morton et al., 2008)* (gift from David Morton); *BcF6-*
251 *GFP* (Tokusumi et al., 2009) (gift from Robert Schulz); *BcF6-mCherry* (Tokusumi et al., 2009),
252 *BcF2-GFP* (Tokusumi et al., 2009); *HmlΔ-DsRed* (Makhijani et al., 2011); and *tubGAL80ts*
253 (McGuire et al., 2003). UAS lines used were *UAS-CD8-GFP* (Song et al., 2007); *UAS-Kir2.1* (Baines
254 et al., 2001) (Bloomington); *UAS-TrpA1* (Bloomington); *UAS-Hid ala5* (Bergmann et al., 2002) (gift
255 from Andreas Bergmann); *UAS-Gyc88E RNAi* (Bloomington). Control lines used were *w1118*
256 (Bloomington) or *yw* (Bloomington). Unless otherwise stated, fly crosses were set and maintained at
257 25° Celsius. Crosses with the driver *Gyc89Db-GAL4* were performed at 29°C to enhance expression.

258 *Hemocyte Quantification*

259 Total hemocyte quantification was performed essentially as described in (Corcoran and Brückner,
260 2020; Petraki et al., 2015). All fluorescently-marked hemocytes of single larvae were released into
261 wells marked by a hydrophobic PAP pen (Beckman Coulter) on glass slides filled with 20-30 μL

262 PBS. Cells were allowed to settle for 15-20 min, and were imaged by fluorescence tile scan
263 microscopy on a Leica DMI4000B microscope with Leica DFC350FX camera and 20x objective.
264 Cell numbers in images were analyzed by particle quantification using Fiji/ImageJ (Corcoran and
265 Brückner, 2020; Petraki et al., 2015; Schindelin et al., 2012).

266 Crystal cell quantification was performed using fluorescent protein reporters or melanization. To
267 quantify crystal cells in live animals, larvae were placed on a slide in a small drop of 10-15 µl PBS
268 with a coverslip on top. Fluorescent crystal cells in each segment were manually counted, rolling the
269 larva by gently moving the coverslip. For phagocytosis lineage tracing, fluorescent crystal cells were
270 quantified ex vivo (see below). To quantify crystal cells based on their ability to melanize (due to
271 their hallmark expression of functional Prophenoloxidase 1 and 2) larvae were placed in 250 µl of
272 PBS in Eppendorf tubes and heated at 65° Celsius for 22 minutes in a heat block, and melanized
273 (black) cells were quantified under a stereoscope by manual counting (Corcoran and Brückner, 2020;
274 Rizki and Rizki, 1959).

275 Larvae were analyzed at various developmental times after egg laying (AEL) corresponding to the
276 following size ranges: 1st instar: ~0.5-1.4mm (22-46h AEL; 2nd instar: ~1.5-2.6mm (47-77h AEL); 3rd
277 instar: ~2.7- >3.5mm (from 78h AEL). For the crosses used, no developmental delays were observed;
278 therefore selection of specified larval size ranges from 24h embryo collections was used in lieu of
279 more tightly timed embryo collections.

280 *Manipulation of Neuronal Activity*

281 To mimic sensory neuron stimulation, larvae were exposed to 10mg/ml carbamylcholine (carbachol,
282 Sigma Aldrich) in fly food for 4 hours allowing direct cuticle contact with carbachol (Makhijani et
283 al., 2017).

284 To activate specific neuron populations, the heat-inducible cation channel TrpA1 was ectopically
285 expressed and transiently heat induced to mimic neuron activation (Hamada et al., 2008).
286 Sopecifically, *TrpA1* crosses were set at RT and shifted to 29°C for 4h. Larvae were analyzed within
287 30 minutes following this period.

288 Sensory neuron silencing was achieved by transiently expressing a transgenic of the inward rectifying
289 potassium channel Kir2.1 (Baines et al., 2001), under control of a sensory neuron specific GAL4
290 driver and a temperature-sensitive GAL4 inhibitor GAL80ts (McGuire et al., 2003); genotypes for
291 neuronal silencing experiments were *21-7-GAL4, UAS-GFP, HmlΔDsRed/UAS-Kir2.1;*

292 *tubGAL80ts/+* with controls *21-7-GAL4, UAS-GFP, HmlΔDsRed/+; tubGAL80ts/+*. F1 from crosses
293 were raised at 18° Celsius. To temporarily silence sensory neurons, larvae were shifted from 18° to
294 29° Celsius for 22 hours to destabilize GAL80ts, allowing for expression of Kir2.1, which
295 hyperpolarizes sensory neuron preventing firing. Larvae were analyzed within 1 hour post-silencing.

296 *Phagocytosis Lineage Tracing*

297 For lineage tracing of crystal cells that derive from actively phagocytic plasmatocytes, larvae with
298 genotype *HmlΔGAL4, UAS-GFP; BcF6-mCherry* were injected with 69 nl of blue fluorescent
299 FluoSphere Carboxylate-modified 0.2 um beads (Invitrogen) diluted 1:100 in PBS using a Nanoject
300 injector (Drummond Scientific). After injection, larvae were placed on food with yeast for 4 hours.
301 Hemocytes of individual larvae were then released into a well marked on a glass slide by PAP pen
302 and filled with 20-30 µl PBS; hemocytes were allowed to settle for 15-20 minutes in a wet chamber
303 (Corcoran and Brückner, 2020; Petraki et al., 2015). Cells were imaged with a Leica DMI4000
304 microscope with tilescan function. Cell quantification was conducted manually from a representative
305 central field of each image (containing ~150-300 plasmatocytes). For genotypes that give rise to
306 substantially reduced numbers of crystal cells, crystal cells of the whole tilescan area were analyzed.
307 Transdifferentiation was quantified by comparing ratios of crystal cells positive for blue particles/
308 total crystal cells (mCherry positive) for various experimental and control conditions. The same
309 quantification for plasmatocytes (GFP positive) with blue beads relative to all plasmatocytes was
310 conducted as an internal control for injection efficiency and phagocytic fitness.

311 *Hypoxia experiments*

312 Hypoxia experiments were conducted using a hypoxic chamber (Biospherix, Inc., Laconia, NY).
313 Oxygen concentrations were set as indicated, supplementing reduced O_2 with N_2. Incubations were
314 performed at room temperature (RT) for 6h. Crystal cell melanization assays were conducted with
315 larvae of the genotype w^{1118}, and phagocytic lineage tracing and total hemocyte experiments used
316 *HmlΔ-GAL4, UAS-GFP; BcF6-mCherry* larvae. For all experiments, 15-25 larvae of the desired
317 age/size and genotype were placed on inactivated yeast paste in cell strainer snap cap tubes, allowing
318 for rapid gas exchange (Corning #352235). Six cell strainer tubes were held by a fitted rack that was
319 inserted into a large cylindrical polystyrene *Drosophila* population cage with steel mesh on one side
320 (custom construction). During transport from the hypoxic chamber to the bench, population cages
321 were sealed in a plastic bag to maintain hypoxic conditions up to the point when larvae were
322 analyzed. Control samples were placed in an identical setup but left at normoxic conditions at

comparable temperature (RT) and time (6h). Following hypoxia/normoxia conditions, assays were conducted as described in the respective paragraphs.

Microscopy

Released hemocytes were imaged on a Leica DMI4000B microscope as described above. Live imaging of larvae was done as described previously, immobilizing larvae on an ice-cooled metal block (Makhijani et al. *Development* 2011). Imaging was performed using a Leica M205FA fluorescent stereoscope with DFC300FX color digital camera and Leica LAS Montage module, combining z-stacks into single in-focus images.

Statistical Analysis

For all experiments numbers of larvae per genotype and condition are indicated in the Figure Legends. For each genotype and condition the mean and standard deviation were determined and significance was tested by 2-way ANOVA (Prism). For hemocyte counts over the course of larval development, regression analysis was performed (Excel). For phagocytosis lineage tracing, the mean and standard deviation of percentages of blue bead positive cells were determined and assessed by 2-way ANOVA (Prism). P-value cutoffs for significance were as follows: * = $p < 0.05$, ** = $p < 0.01$, and *** = $p < 0.001$. Pools of both male and female larvae were analyzed.

Authors' contributions

KB conceived and supervised the study. SC, AM and KB planned the experiments. SC, AM, JA, YH, DO, TJ, KK carried out the experiments. SC, AM, JA, YH, DO, TJ, KK and KB analyzed the data. KB wrote the manuscript with input from all authors.

Competing interests

The authors have no competing interests.

Funding

This work was supported by grants from the American Cancer Society RSG DDC-122595, American Heart Association 13BGIA13730001, National Science Foundation 1326268, and National Institutes of Health 1R01GM112083, 1R56HL118726 and 1R01GM131094 (to KB).

Acknowledgements

We thank D. Morton, R. Schulz, U. Banerjee, A. Bergmann, C. Evans, D. Hultmark, Y.N. Jan, L. Kockel, the Bloomington Stock Center, and TRiP for fly stocks. We are grateful to Khalida Sabeur and Manideep Chavali for help to access and use hypoxia chamber equipment. Thanks to Ava Brückner-Kockel for advice on regression analysis. We thank members of the Brückner lab for discussion and feedback on the manuscript.

357 **References**

358

359 Baines, R.A., Uhler, J.P., Thompson, A., Sweeney, S.T., and Bate, M. (2001). Altered electrical
360 properties in *Drosophila* neurons developing without synaptic transmission. J Neurosci *21*, 1523-
361 1531.

362 Banerjee, U., Girard, J.R., Goins, L.M., and Spratford, C.M. (2019). *Drosophila* as a Genetic Model
363 for Hematopoiesis. Genetics *211*, 367-417.

364 Bergmann, A., Tugentman, M., Shilo, B.Z., and Steller, H. (2002). Regulation of cell number by
365 MAPK-dependent control of apoptosis: a mechanism for trophic survival signaling. Dev Cell *2*, 159-
366 170.

367 Bidla, G., Hauling, T., Dushay, M.S., and Theopold, U. (2009). Activation of insect phenoloxidase
368 after injury: endogenous versus foreign elicitors. J Innate Immun *1*, 301-308.

369 Caravagna, C., and Seaborn, T. (2016). Oxygen Sensing in Early Life. Lung *194*, 715-722.

370 Cevik, D., Acker, M., Michalski, C., and Jacobs, J.R. (2019). Pericardin, a *Drosophila* collagen,
371 facilitates accumulation of hemocytes at the heart. Dev Biol *454*, 52-65.

372 Chabi, S., Uzan, B., Naguibneva, I., Rucci, J., Fahy, L., Calvo, J., Arcangeli, M.L., Mazurier, F.,
373 Pflumio, F., and Haddad, R. (2019). Hypoxia Regulates Lymphoid Development of Human
374 Hematopoietic Progenitors. Cell Rep *29*, 2307-2320 e2306.

375 Chang, R.B., Strochlic, D.E., Williams, E.K., Umans, B.D., and Liberles, S.D. (2015). Vagal Sensory
376 Neuron Subtypes that Differentially Control Breathing. Cell *161*, 622-633.

377 Cieslar-Pobuda, A., Knoflach, V., Ringh, M.V., Stark, J., Likus, W., Siemianowicz, K., Ghavami, S.,
378 Hudecki, A., Green, J.L., and Los, M.J. (2017). Transdifferentiation and reprogramming: Overview
379 of the processes, their similarities and differences. Biochim Biophys Acta Mol Cell Res *1864*, 1359-
380 1369.

381 Cirovic, B., Schonheit, J., Kowenz-Leutz, E., Ivanovska, J., Klement, C., Pronina, N., Begay, V., and
382 Leutz, A. (2017). C/EBP-Induced Transdifferentiation Reveals Granulocyte-Macrophage Precursor-
383 like Plasticity of B Cells. Stem Cell Reports *8*, 346-359.

384 Collombet, S., van Oevelen, C., Sardina Ortega, J.L., Abou-Jaoude, W., Di Stefano, B., Thomas-
385 Chollier, M., Graf, T., and Thieffry, D. (2017). Logical modeling of lymphoid and myeloid cell
386 specification and transdifferentiation. Proc Natl Acad Sci U S A *114*, 5792-5799.

387 Corcoran, S., and Brückner, K. (2020). Quantification of blood cells in *Drosophila* and other insects.
388 Springer Protocols Handbooks: Immunity in Insects *Sandrelli F, Tettamanti G, editors*, 65-77.

389 Cutz, E., Yeger, H., and Pan, J. (2007). Pulmonary neuroendocrine cell system in pediatric lung
390 disease-recent advances. Pediatr Dev Pathol *10*, 419-435.

391 Davies, L.C., Jenkins, S.J., Allen, J.E., and Taylor, P.R. (2013). Tissue-resident macrophages. Nat
392 Immunol *14*, 986-995.

393 Di Tullio, A., Vu Manh, T.P., Schubert, A., Castellano, G., Mansson, R., and Graf, T. (2011).
394 CCAAT/enhancer binding protein alpha (C/EBP(alpha))-induced transdifferentiation of pre-B cells
395 into macrophages involves no overt retrodifferentiation. Proc Natl Acad Sci U S A *108*, 17016-
396 17021.

397 Ding, X.B., Jin, J., Tao, Y.T., Guo, W.P., Ruan, L., Yang, Q.L., Chen, P.C., Yao, H., Zhang, H.B.,
398 and Chen, X. (2020). Predicted *Drosophila* Interactome Resource and web tool for functional
399 interpretation of differentially expressed genes. Database (Oxford) *2020*.

400 Dudzic, J.P., Kondo, S., Ueda, R., Bergman, C.M., and Lemaitre, B. (2015). *Drosophila* innate
401 immunity: regional and functional specialization of prophenoloxidases. BMC Biol *13*, 81.

402 Duvic, B., Hoffmann, J.A., Meister, M., and Royet, J. (2002). Notch signaling controls lineage
403 specification during *Drosophila* larval hematopoiesis. Curr Biol *12*, 1923-1927.

404 Gold, K.S., and Brückner, K. (2014). *Drosophila* as a model for the two myeloid blood cell systems
405 in vertebrates. Exp Hematol *42*, 717-727.

406 Gold, K.S., and Brückner, K. (2015). Macrophages and cellular immunity in *Drosophila*
407 *melanogaster*. Semin Immunol *27*, 357-368.

408 Gorr, T.A., Gassmann, M., and Wappner, P. (2006). Sensing and responding to hypoxia via HIF in
409 model invertebrates. J Insect Physiol *52*, 349-364.

410 Graf, T. (2011). Historical origins of transdifferentiation and reprogramming. Cell Stem Cell *9*, 504-
411 516.

412 Haase, V.H. (2013). Regulation of erythropoiesis by hypoxia-inducible factors. Blood Rev *27*, 41-53.

413 Hamada, F.N., Rosenzweig, M., Kang, K., Pulver, S.R., Ghezzi, A., Jegla, T.J., and Garrity, P.A.
414 (2008). An internal thermal sensor controlling temperature preference in *Drosophila*. Nature *454*,
415 217-220.

416 Hanoun, M., Maryanovich, M., Arnal-Estape, A., and Frenette, P.S. (2015). Neural regulation of
417 hematopoiesis, inflammation, and cancer. Neuron *86*, 360-373.

418 Hayashi, S., and Kondo, T. (2018). Development and Function of the *Drosophila* Tracheal System.
419 Genetics *209*, 367-380.

420 Holz, A., Bossinger, B., Strasser, T., Janning, W., and Klapper, R. (2003). The two origins of
421 hemocytes in *Drosophila*. Development *130*, 4955-4962.

422 Huang, S.H., Rio, D.C., and Marletta, M.A. (2007). Ligand binding and inhibition of an oxygen-
423 sensitive soluble guanylate cyclase, Gyc-88E, from *Drosophila*. Biochemistry *46*, 15115-15122.

424 Imanirad, P., and Dzierzak, E. (2013). Hypoxia and HIFs in regulating the development of the
425 hematopoietic system. Blood Cells Mol Dis *51*, 256-263.

426 Inokuchi, K., Kato, A., Hiraia, K., Hishinuma, F., Inoue, M., and Ozawa, F. (1996). Increase in
427 activin beta A mRNA in rat hippocampus during long-term potentiation. FEBS Lett *382*, 48-52.

428 Kaupp, U.B., and Seifert, R. (2002). Cyclic nucleotide-gated ion channels. Physiol Rev *82*, 769-824.

429 Krzemien, J., Dubois, L., Makki, R., Meister, M., Vincent, A., and Crozatier, M. (2007). Control of
430 blood cell homeostasis in *Drosophila* larvae by the posterior signalling centre. Nature *446*, 325-328.

431 Kuhn, D.T., Sawyer, M., Packert, G., Turenchalk, G., Mack, J.A., Sprey, T.E., Gustavson, E., and
432 Kornberg, T.B. (1992). Development of the D. *melanogaster* caudal segments involves suppression
433 of the ventral regions of A8, A9 and A10. Development *116*, 11-20.

434 Kumar, A., and Brockes, J.P. (2012). Nerve dependence in tissue, organ, and appendage regeneration.
435 Trends in neurosciences *35*, 691-699.

436 Lanot, R., Zachary, D., Holder, F., and Meister, M. (2001). Postembryonic hematopoiesis in
437 *Drosophila*. Dev Biol *230*, 243-257.

438 Lebestky, T., Chang, T., Hartenstein, V., and Banerjee, U. (2000). Specification of *Drosophila*
439 hematopoietic lineage by conserved transcription factors. Science *288*, 146-149.

440 Lebestky, T., Jung, S.H., and Banerjee, U. (2003). A Serrate-expressing signaling center controls
441 *Drosophila* hematopoiesis. Genes Dev *17*, 348-353.

442 Lefrancais, E., Ortiz-Munoz, G., Caudrillier, A., Mallavia, B., Liu, F., Sayah, D.M., Thornton, E.E.,
443 Headley, M.B., David, T., Coughlin, S.R.*, et al.* (2017). The lung is a site of platelet biogenesis and a
444 reservoir for haematopoietic progenitors. Nature *544*, 105-109.

445 Leitao, A.B., and Sucena, E. (2015). *Drosophila* sessile hemocyte clusters are true hematopoietic
446 tissues that regulate larval blood cell differentiation. Elife *4*.

447 Li, P., Burke, S., Wang, J., Chen, X., Ortiz, M., Lee, S.C., Lu, D., Campos, L., Goulding, D., Ng,
448 B.L.*, et al.* (2010). Reprogramming of T cells to natural killer-like cells upon Bcl11b deletion.
449 Science *329*, 85-89.

450 Lu, A., Zhang, Q., Zhang, J., Yang, B., Wu, K., Xie, W., Luan, Y.X., and Ling, E. (2014). Insect
451 prophenoloxidase: the view beyond immunity. Front Physiol *5*, 252.

452 Majmundar, A.J., Wong, W.J., and Simon, M.C. (2010). Hypoxia-inducible factors and the response
453 to hypoxic stress. Mol Cell *40*, 294-309.

454 Makhijani, K., Alexander, B., Rao, D., Petraki, S., Herboso, L., Kukar, K., Batool, I., Wachner, S.,
455 Gold, K.S., Wong, C.*, et al.* (2017). Regulation of *Drosophila* hematopoietic sites by Activin-beta
456 from active sensory neurons. Nat Commun *8*, 15990.

457 Makhijani, K., Alexander, B., Tanaka, T., Rulifson, E., and Brückner, K. (2011). The peripheral
458 nervous system supports blood cell homing and survival in the *Drosophila* larva. Development *138*,
459 5379-5391.

460 Makhijani, K., and Brückner, K. (2012). Of blood cells and the nervous system: Hematopoiesis in the
461 *Drosophila* larva. Fly (Austin) *6*, 254-260.

462 Markus, R., Laurinyecz, B., Kurucz, E., Honti, V., Bajusz, I., Sipos, B., Somogyi, K., Kronhamn, J.,
463 Hultmark, D., and Ando, I. (2009). Sessile hemocytes as a hematopoietic compartment in *Drosophila*
464 *melanogaster*. Proc Natl Acad Sci U S A *106*, 4805-4809.

465 Martin, J.F., Slater, D.N., and Trowbridge, E.A. (1983). Abnormal intrapulmonary platelet
466 production: a possible cause of vascular and lung disease. Lancet *1*, 793-796.

467 Mazzone, S.B., and Undem, B.J. (2016). Vagal Afferent Innervation of the Airways in Health and
468 Disease. Physiol Rev *96*, 975-1024.

469 McGuire, S.E., Le, P.T., Osborn, A.J., Matsumoto, K., and Davis, R.L. (2003). Spatiotemporal rescue
470 of memory dysfunction in *Drosophila*. Science *302*, 1765-1768.

471 Miyashita, T., Oda, Y., Horiuchi, J., Yin, J.C., Morimoto, T., and Saitoe, M. (2012). Mg(2+) block of
472 *Drosophila* NMDA receptors is required for long-term memory formation and CREB-dependent gene
473 expression. Neuron *74*, 887-898.

474 Morton, D.B. (2004). Atypical soluble guanylyl cyclases in *Drosophila* can function as molecular
475 oxygen sensors. J Biol Chem *279*, 50651-50653.

476 Morton, D.B., Langlais, K.K., Stewart, J.A., and Vermehren, A. (2005). Comparison of the properties
477 of the five soluble guanylyl cyclase subunits in *Drosophila melanogaster*. J Insect Sci *5*, 12.

478 Morton, D.B., Stewart, J.A., Langlais, K.K., Clemens-Grisham, R.A., and Vermehren, A. (2008).
479 Synaptic transmission in neurons that express the *Drosophila* atypical soluble guanylyl cyclases,
480 Gyc-89Da and Gyc-89Db, is necessary for the successful completion of larval and adult ecdysis. J
481 Exp Biol *211*, 1645-1656.

482 Mukherjee, T., Kim, W.S., Mandal, L., and Banerjee, U. (2011). Interaction between Notch and Hif-
483 alpha in development and survival of *Drosophila* blood cells. Science *332*, 1210-1213.

484 Pavlov, V.A., and Tracey, K.J. (2012). The vagus nerve and the inflammatory reflex--linking
485 immunity and metabolism. Nature reviews Endocrinology *8*, 743-754.

486 Perdiguero, E.G., and Geissmann, F. (2016). The development and maintenance of resident
487 macrophages. Nat Immunol *17*, 2-8.

488 Pesaresi, M., Sebastian-Perez, R., and Cosma, M.P. (2019). Dedifferentiation, transdifferentiation and
489 cell fusion: in vivo reprogramming strategies for regenerative medicine. Febs J *286*, 1074-1093.

490 Petraki, S., Alexander, B., and Brückner, K. (2015). Assaying Blood Cell Populations of the
491 *Drosophila melanogaster* Larva. J Vis Exp.

492 Pifferi, S., Boccaccio, A., and Menini, A. (2006). Cyclic nucleotide-gated ion channels in sensory
493 transduction. FEBS Lett *580*, 2853-2859.

494 Pokorski, M., Takeda, K., and Okada, Y. (2016). Oxygen Sensing Mechanisms: A Physiological
495 Penumbra. Adv Exp Med Biol *952*, 1-8.

496 Rapino, F., Robles, E.F., Richter-Larrea, J.A., Kallin, E.M., Martinez-Climent, J.A., and Graf, T.
497 (2013). C/EBPalpha induces highly efficient macrophage transdifferentiation of B lymphoma and
498 leukemia cell lines and impairs their tumorigenicity. Cell Rep *3*, 1153-1163.

499 Reid, A., and Tursun, B. (2018). Transdifferentiation: do transition states lie on the path of
500 development? Curr Opin Syst Biol *11*, 18-23.

501 Rizki, M.T., and Rizki, R.M. (1959). Functional significance of the crystal cells in the larva of
502 *Drosophila melanogaster*. J Biophys Biochem Cytol *5*, 235-240.

503 Schindelin, J., Arganda-Carreras, I., Frise, E., Kaynig, V., Longair, M., Pietzsch, T., Preibisch, S.,
504 Rueden, C., Saalfeld, S., Schmid, B*., et al.* (2012). Fiji: an open-source platform for biological-image
505 analysis. Nat Methods *9*, 676-682.

506 Sieweke, M.H., and Allen, J.E. (2013). Beyond stem cells: self-renewal of differentiated
507 macrophages. Science *342*, 1242974.

508 Sinenko, S.A., and Mathey-Prevot, B. (2004). Increased expression of *Drosophila* tetraspanin,
509 Tsp68C, suppresses the abnormal proliferation of ytr-deficient and Ras/Raf-activated hemocytes.
510 Oncogene *23*, 9120-9128.

511 Siripin, D., Kheolamai, P., Y, U.P., Supokawej, A., Wattanapanitch, M., Klincumhom, N.,
512 Laowtammathron, C., and Issaragrisil, S. (2015). Transdifferentiation of erythroblasts to
513 megakaryocytes using FLI1 and ERG transcription factors. Thromb Haemost *114*, 593-602.

514 Song, W., Onishi, M., Jan, L.Y., and Jan, Y.N. (2007). Peripheral multidendritic sensory neurons are
515 necessary for rhythmic locomotion behavior in *Drosophila* larvae. Proc Natl Acad Sci U S A *104*,
516 5199-5204.

517 Stewart, S., Koh, T.W., Ghosh, A.C., and Carlson, J.R. (2015). Candidate ionotropic taste receptors
518 in the *Drosophila* larva. Proc Natl Acad Sci U S A *112*, 4195-4201.

519 Tattikota, S.G., Hu, Y., Liu, Y., Cho, B., Barrera, V., Steinbaugh, M., Yoon, S.-H., Comjean, A., Li,
520 F., Dervis, F.*, et al.* (2019). A single-cell survey of *Drosophila* blood. bioRxiv,
521 2019.2012.2020.884999.

522 Tokusumi, T., Shoue, D.A., Tokusumi, Y., Stoller, J.R., and Schulz, R.A. (2009). New hemocyte-
523 specific enhancer-reporter transgenes for the analysis of hematopoiesis in *Drosophila*. Genesis *47*,
524 771-774.

525 Vermehren, A., Langlais, K.K., and Morton, D.B. (2006). Oxygen-sensitive guanylyl cyclases in
526 insects and their potential roles in oxygen detection and in feeding behaviors. J Insect Physiol *52*,
527 340-348.

528 Vermehren-Schmaedick, A., Ainsley, J.A., Johnson, W.A., Davies, S.A., and Morton, D.B. (2010).
529 Behavioral responses to hypoxia in *Drosophila* larvae are mediated by atypical soluble guanylyl
530 cyclases. Genetics *186*, 183-196.

531 Vermehren-Schmaedick, A., Scudder, C., Timmermans, W., and Morton, D.B. (2011). *Drosophila*
532 gustatory preference behaviors require the atypical soluble guanylyl cyclases. J Comp Physiol A
533 Neuroethol Sens Neural Behav Physiol *197*, 717-727.

534 Wingrove, J.A., and O'Farrell, P.H. (1999). Nitric oxide contributes to behavioral, cellular, and
535 developmental responses to low oxygen in *Drosophila*. Cell *98*, 105-114.

536 Wu, Q., Wen, T., Lee, G., Park, J.H., Cai, H.N., and Shen, P. (2003). Developmental control of
537 foraging and social behavior by the *Drosophila* neuropeptide Y-like system. Neuron *39*, 147-161.

538 Xiang, Y., Yuan, Q., Vogt, N., Looger, L.L., Jan, L.Y., and Jan, Y.N. (2010). Light-avoidance-
539 mediating photoreceptors tile the *Drosophila* larval body wall. Nature *468*, 921-926.

540 Xie, H., Ye, M., Feng, R., and Graf, T. (2004). Stepwise reprogramming of B cells into macrophages.
541 Cell *117*, 663-676.

542 Yang, H., Kronhamn, J., Ekstrom, J.O., Korkut, G.G., and Hultmark, D. (2015). JAK/STAT signaling
543 in *Drosophila* muscles controls the cellular immune response against parasitoid infection. EMBO
544 Rep *16*, 1664-1672.

545

546 **Figure Legends**

547

548 **Figure 1. Crystal cells in the *Drosophila* larva are generated by transdifferentiation**

549 (A) Development of crystal cell numbers over time. Crystal cells per larva, assessed by melanization,
550 relative to larval size and developmental stage. Genotype is w^{1118}, n=155. Mean and standard
551 deviation, regression analysis.

552 (B) Development of total hemocyte numbers over time. Total hemocytes per larva, genotype is
553 *HmlΔGAL4, UAS-GFP; He-GAL4*; n=107. Mean and standard deviation, regression analysis.

554 (C-C'') Localization of plasmatocytes and crystal cells in the 3rd instar larva,; genotype is *BcF2-GFP/*
555 *Hml*Δ*-DsRed*; plasmatocytes labeled by *Hml*Δ*-DsRed* (red); crystal cells labeled by *BcF2-GFP*
556 (green); lateral view, posterior right.

557 (D-D') Model of distribution of plasmatocyte (red) and crystal cells (orange) in *Drosophila* larva,
558 relevant sensory neuron clusters of the hematopoietic pockets (green); lateral view, posterior right.

559 (E-E''') Scheme of phagocytosis lineage tracing assay. Blue fluorescent latex beads are injected into
560 early 3rd instar larvae, cells are released after indicated incubation times; fraction of cells containing
561 phagocytosed beads are determined. Possible outcomes are depicted with crystal cells in orange,
562 plasmatocytes in red, progenitors in grey.

563 (F) Sample image of analyzed cells; genotype *BcF2-GFP/ Hml*Δ*-DsRed*; crystal cells in green,
564 plasmatocytes in red; blue arrowheads indicate crystal cells with incorporated blue beads.

565 (G) Quantification of samples as in (G); fraction of plasmatocytes and crystal cells containing blue
566 beads at time 1h, 4, 22h after injection; n=21; mean and standard deviation.

567

568 **Figure 2. Sensory Neuron activity regulates transdifferentiation to crystal cells**

569 (A) Plasmatocytes colocalize with sensory neurons in all hematopoietic pockets; genotype *21-7-*
570 *GAL4, UAS-CD8-GFP, Hml*Δ*DsRed/CyO* ; lateral view, posterior right.

571 (B) Crystal cells also colocalize with sensory neurons but are mainly found in a cluster at the caudal
572 end of the larva; genotype *21-7-GAL4, UAS-CD8-GFP/+; BCF6-mCherry/*+; lateral view, posterior
573 right.

574 (C) Treatment of larvae with the AchR agonist carbachol to mimic sensory neuron activation,
575 treatment for 4h; genotype is *yw*; quantification of crystal cells by melanization; control n=65 (+45);
576 carbachol n=34 (+50). Individual value plot with mean and standard deviation, two-way ANOVA.

577 (D) Transient silencing of sensory neurons, quantification of crystal cells by melanization; genotypes
578 are experiment *21-7-GAL4, UAS-CD8GFP, Hml*Δ*-DsRed/ UAS-Kir2.1; tubGAL80ts/* + and control
579 *21-7-GAL4, UAS-CD8GFP, Hml*Δ*-DsRed/ +; tubGAL80ts/* +. Larvae induced at 29˚C for 22h. Mean
580 and standard deviation, two-way ANOVA.

581 (E, F) Phagocytosis lineage tracing, genotypes are experiment *21-7-GAL4, UAS-CD8GFP, Hml*Δ-
582 *DsRed/ UAS-Kir2.1; BcF6-GFP/ tubGAL80ts*, and control *21-7-GAL4, UAS-CD8GFP, Hml*Δ*-DsRed/*
583 *+; BcF6-GFP/ tubGAL80ts*.

584 (E) Sample image of analyzed cells, plasmatocytes (red), crystal cells (green), injected beads (blue).

585 (F) Quantification of samples as in (E); fraction of plasmatocytes and crystal cells containing blue
586 beads, experiment n=12 and control n=12. Mean and standard deviation, two-way ANOVA.

587

588 **Figure 3. Crystal cells are clustered around the sensory cones and are promoted by sensory**
589 **cone neurons**

590 (A-D) Localization of sensory neurons, plasmatocytes and crystal cells, caudal view of larvae; scale
591 bars 0.25mm.

592 (A) Sensory neurons (green), genotype *21-7-GAL4, UAS-CD8-GFP, Hml*Δ*-DsRed/CyO*; 3rd instar
593 larva.

594 (B) Plasmatocytes (green) and crystal cells (red), genotype *Hml*Δ*-GAL4, UAS-GFP; BcF6-mCherry*;
595 2nd instar larva.

596 (C) Crystal cells (red) and sensory neurons (green), genotype *21-7-GAL4, UAS-CD8-GFP/+; BcF6-*
597 *mCherry/*+; 2nd instar larva.

598 (D) Crystal cells (red) and sensory neurons (green), *21-7-GAL4, UAS-CD8-GFP/+; BcF6-*
599 *mCherry/*+; 3rd instar larva.

600 (A'-D') Models corresponding to (A-D), respectively, plasmatocytes red, crystal cells orange,
601 sensory neurons green; caudal view.

602 (A''-D'') Models, lateral view, corresponding to (A-C and A'-C'), respectively; lateral view.

603 (E) *Gyc89Db-GAL4* driver expressing GFP in sensory cone neurons (green), lateral view, genotype is
604 *UAS-GFP/+; Gyc89Db-GAL4/+*; lateral view, posterior right; scale bar 0.5mm.

605 (F) Larva as in (E), caudal view.

606 (G) Ablation of sensory cone neurons affects crystal cells; quantification of crystal cells per larva by
607 melanization. Genotypes are experiment *UAS-Hid ala5/+; Gyc89Db-GAL4/tubGAL80ts*, n=34 and
608 control *Gyc89Db-GAL4/tubGAL80ts*, n=34. Crosses were raised at 18˚C and temperature shifted to
609 29 ˚C for 16 h. Individual value plot with mean and standard deviation, two-way ANOVA.

610 (H) Transient activation of TrpA1 in sensory cone neurons; quantification of crystal cells per larva by
611 melanization. Genotypes are experiment *UAS-TrpA1/ +; Gyc89Db-GAL4, / +*, n=46, and control
612 *Gyc89Db-GAL4/+*, n=48*;* in addition, one experiment F1 cohort *UAS-TrpA1/ +; Gyc89Db-GAL4, /*
613 *+*, n=47, was maintained as uninduced control at RT. Crosses were raised at RT and temperature
614 shifted to 29˚C for 4 hours;. Individual value plot with mean and standard deviation, two-way
615 ANOVA.

616

617 **Figure 4. Oxygen sensing through Gycs in sensory cone neurons drives plasmatocyte-to-crystal**
618 **cell transdifferentiation**

619 (A) RNAi silencing of *Gyc88E* in sensory cone neurons results in reduced crystal cell numbers
620 determined by melanization; genotyes are experiment *Gyc89Db-GAL4/UAS-Gyc88ERNAi*, n=45 and
621 control *Gyc89Db-GAL4/+*. n=45. Individual value plot with mean and standard deviation, two-way
622 ANOVA.

623 (B) Phagocytosis lineage tracing, effect of *Gyc88E* RNAi in sensory cone neurons on
624 transdifferentiation; genotypes are experiment *21-7-GAL4, UA5-CD8-GFP, Hml*Δ*-DsRed/+; BcF6-*
625 *GFP/ UAS-Gyc88ERNAi*, n=11 and control *21-7-GAL4, UA5-CD8-GFP, Hml*Δ*-DsRed/+; BcF6-*
626 *GFP/+*, n=16. Bar chart with mean and standard deviation, two-way ANOVA.

627 (C) Effect of hypoxia (5% O2) on crystal cell number per larva determined by melanization;
628 genotype is w^{1118}; hypoxia n=46 and normoxia n=48. Individual value plot with mean and standard
629 deviation, two-way ANOVA.

630 (D) Phagocytosis lineage tracing, effect of hypoxia (5% O2) on transdifferentiation; genotype is
631 *Hml*Δ*-GAL4, UAS-GFP; BcF6-mCherry*; hypoxia n=14 and normoxia n=15. Bar chart with mean and
632 standard deviation, two-way ANOVA.

633 (E) Model. Sensory cone neurons require oxygen and cytoplasmic Gyc88E to drive crystal cell
634 formation. Gyc88E converts GTP to cGMP, leading to downstream signaling and neuronal activation.
635 Through a currently unknown mechanism, long-term hypoxia negatively affects this process. Active
636 neurons induce plasmatocyte-to-crystal cell transdifferentiation.

637

638

639

640

641 **Supplemental Information**

642

643 **Supplemental Figure 1. Methods of crystal cell labeling**

644 (A) Heat induced melanization of crystal cells. Genotype is *lz-GAL4;UAS-GFP*

645 (B) Fluorescent reporter labeling to visualize, and quantify, crystal cells. Genotype is *lz-GAL4;UAS-*
646 *GFP*. Note that the labeled crystal cell pattern by both methods is very similar.

647

648 **Supplemental Figure 2. Limited transient sensory neuron silencing does not affect total**
649 **hemocyte numbers**

650 (A) Transient silencing of sensory neurons, quantification of total hemocytes; genotypes are *21-7-*
651 *GAL4, UAS-CD8-GFP, Hml*Δ*-DsRed/ UAS-Kir2.1; tubGAL80ts/* + , n=12 and control *21-7-GAL4,*
652 *UAS-CD8-GFP, Hml*Δ*-DsRed/ +; tubGAL80ts/* +, n=13. Larvae induced at 29˚C for 22h. Mean and
653 standard deviation, two-way ANOVA

654

655 **Supplemental Figure 3. Hypoxia affects crystal cell counts but not total hemocyte numbers**

656 (A) Effect of 8% hypoxia on crystal cell number determined by melanization; genotype is *w1118*;
657 hypoxia n=19 and normoxia control n=18. Individual value plot with mean and standard deviation,
658 two-way ANOVA.

659 (B) Total hemocyte number under conditions of hypoxia (5% O2) and normoxia; genotype is *Hml*Δ-
660 *GAL4, UAS-GFP; BcF6-mCherry*; hypoxia n=14 and normoxia control n=14. Mean and standard
661 deviation, two-way ANOVA.

662

663 **Supplemental Figure 4. Models**

664 (A) In the presence of oxygen, active sensory cone neurons produce signal/s that drive
665 transdifferentiation of plasmatocytes to crystal cells. According to this model, transdifferentiation is
666 triggered by a, likely secreted, sensory neuron signal, therefore plasmatocytes in anatomical
667 proximity to the sensory cone neurons are most likely to convert to crystal cells.

668 (B) Model illustrating exposure of the caudal end of *Drosophila* larvae including the sensory cones
669 and posterior spiracles to the air, while burying in food. Mature larvae leave the food in preparation
670 of pupariation, now fully exposed to the air.

671

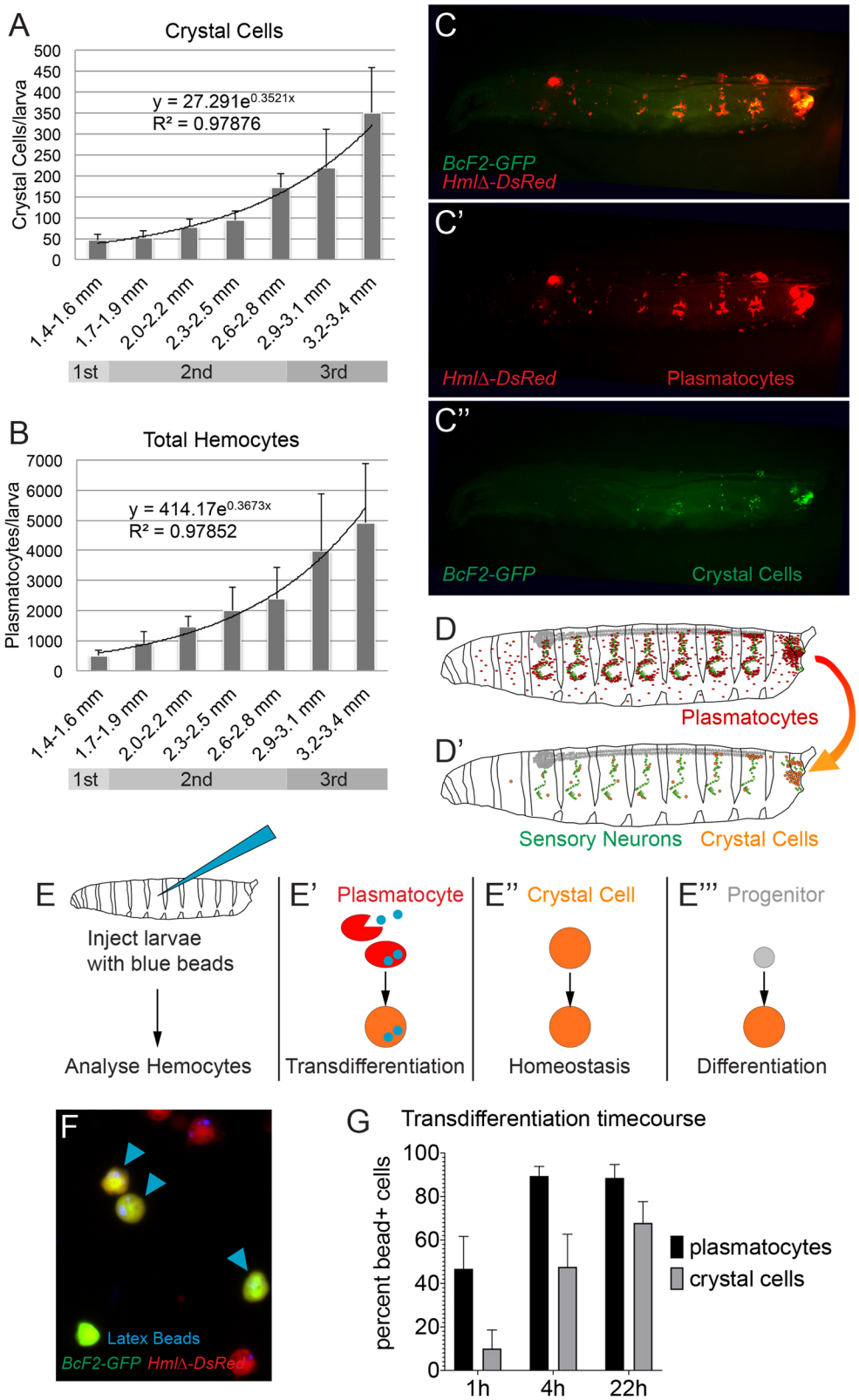

Corcoran et al., Figure 1

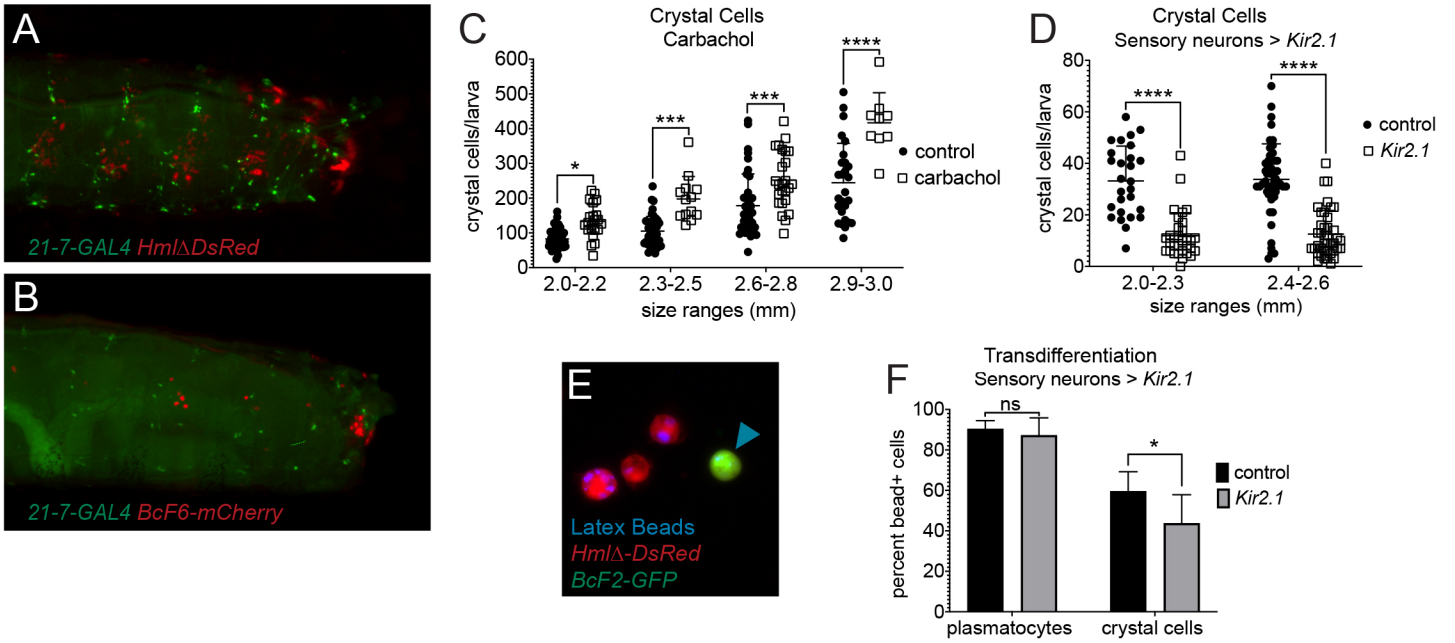

Corcoran et al. Figure 2

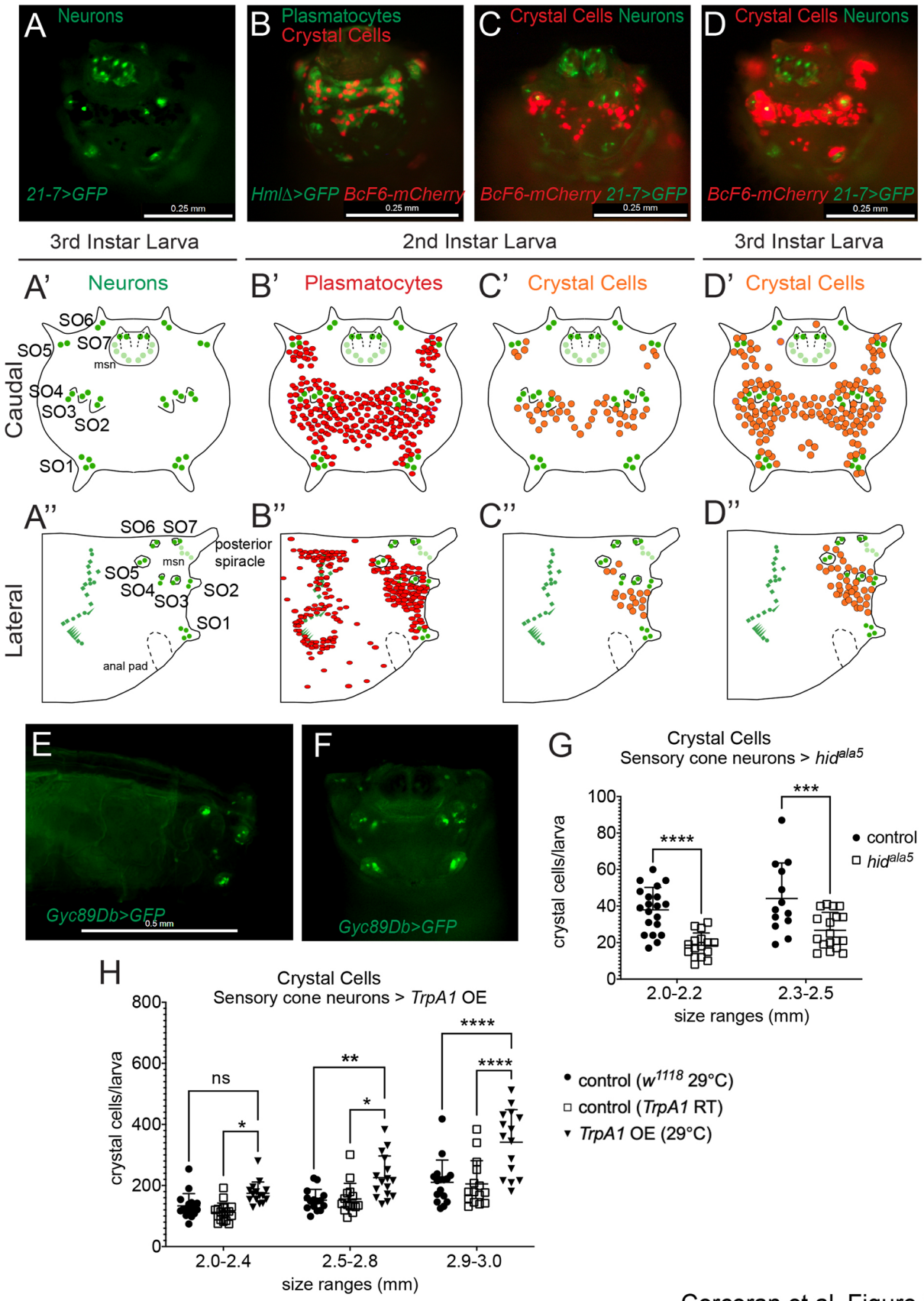

Corcoran et al. Figure 3

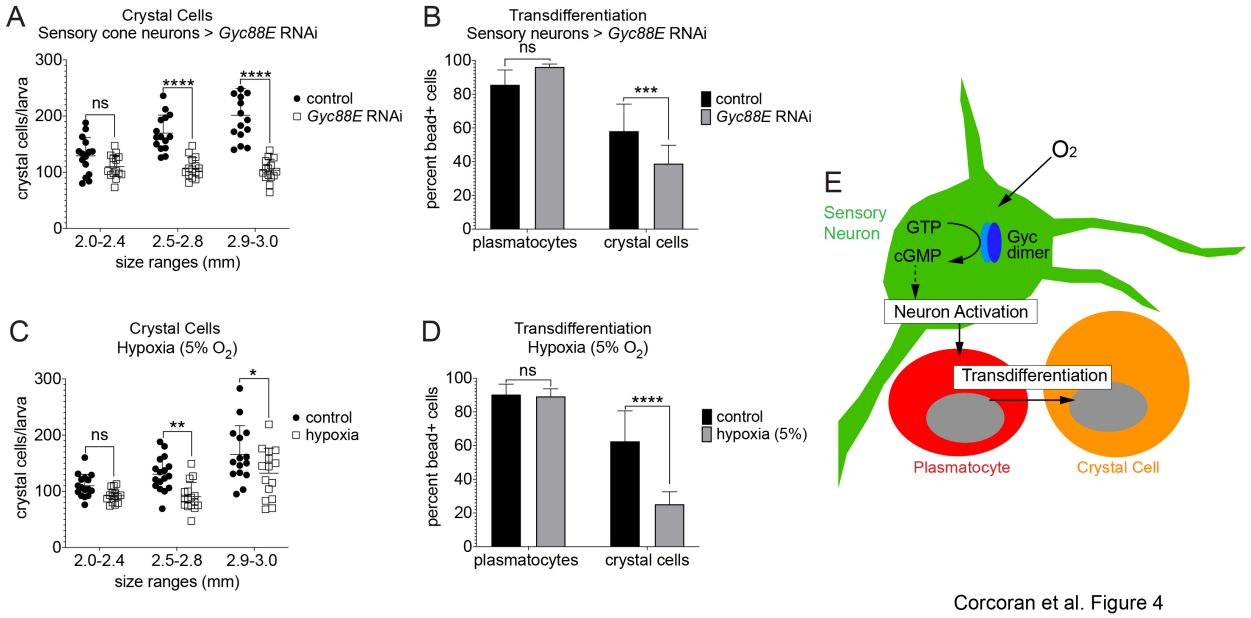

Corcoran et al. Figure 4

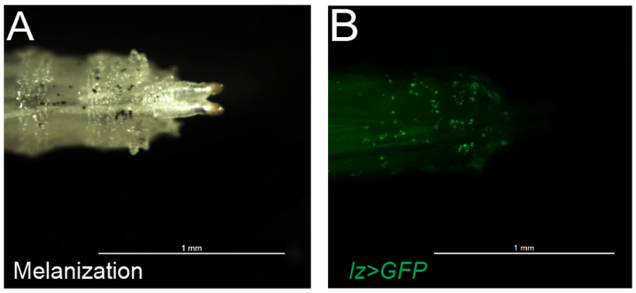

Corcoran et al. Supplemental Figure 1

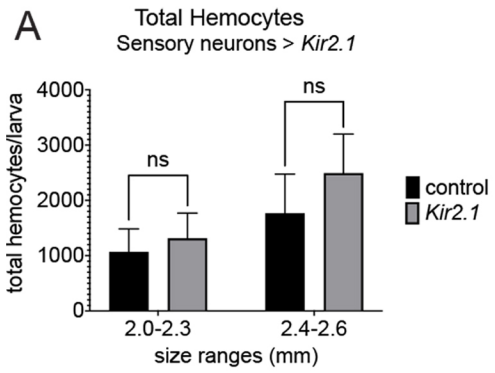

Corcoran et al. Supplemental Figure 2

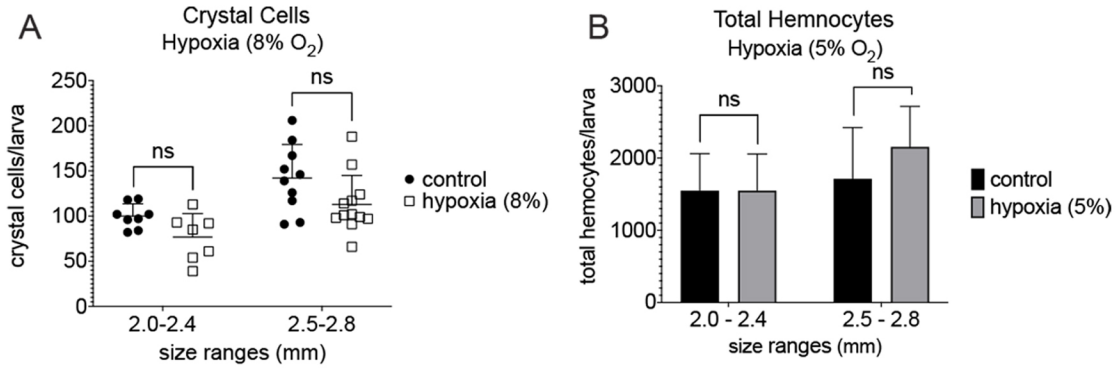

Corcoran et al. Supplemental Figure 3

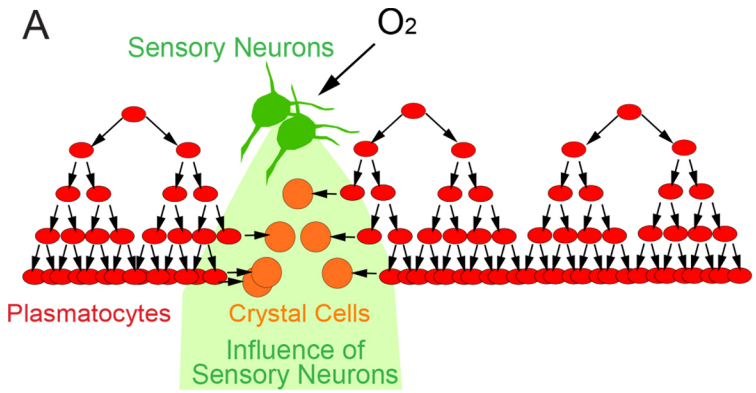

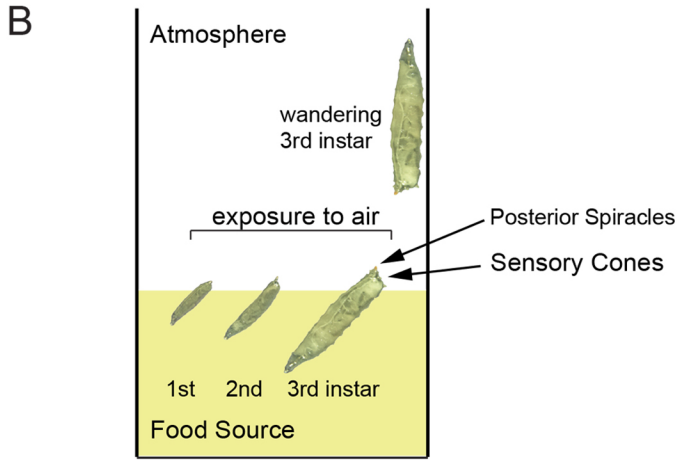

Corcoran et al. Supplemental Figure 4